IoT cloud-based Power Quality extended functionality for Grid-Interactive Appliance Controllers

Joaquin Garrido-Zafra, *Student Member*, *IEEE*, Aurora Gil-de-Castro, *Senior Member*, *IEEE*, Rafael Savariego-Fernandez, Matias Linan-Reyes, Felix Garcia-Torres and Antonio Moreno-Munoz, Senior Member, IEEE.

***Abstract*—Due to the myriad of loads that are collected into commercial Grid-interactive Efficient Buildings (GEBs) focused on the industry 4.0 paradigm, it is important to ensure their proper electrical operation. The power quality (PQ) here requires a granular monitoring approach, reaching a point where each device connected to the microgrid can diagnose whether its power supply is optimal. Otherwise, it can participate cooperatively in decision-making to avoid anomalies or faults in the microgrid. In this work, we present cloud-based extended functionality to make smart appliances (SA) responsive to the grid, either autonomously or managed under the open automated demand response (OpenADR) standard. Further to acting as a switch, the main strength lies in its PQ monitoring via the Fiware Internet of Things (IoT) platform with data-driven analytics capabilities. It identifies and even predicts a broad spectrum of electrical disturbances, far exceeding the capabilities of previous solutions such as the grid-friendly appliance controller, so it is possible to customize a battery of alarms at will (e.g., according to IEEE 1547 standard). Moreover, although it can act autonomously, its main mission will be to act in a coordinated manner, either cooperatively or under the supervision of the GEB Energy Management System (EMS). Finally, different case studies are presented to show their capabilities. With the integration of these distributed sub-metering systems, under standards IoT wireless communication protocols, a further step will be taken in the advent of the digital utility paradigm.**

***Index Terms*—advanced metering infrastructure, Demand Response, Fiware, grid friendly appliance, grid-interactive appliance, internet of things, OpenADR, power quality, smart appliances, smart grids.**

I. Introduction

The market for large household appliances is expected to grow annually by 1.8% (CAGR 2019-2023), reaching 368 billion dollars in 2023 [1]. This increasing pace is being driven by several trends, such as the expansion of digitization in everyday life, the citizen interest in sustainability, and the increase in the purchasing power of the average consumer. Meeting these expectations requires investments and economies of scale, but on the other hand, it can bring new opportunities for innovation. Thus, in recent years we have witnessed the appearance and proliferation of SAs. Popularly SAs are recognized for having some electronic processing capability and wireless connectivity. For example, smart washing machines can independently regulate the washing powder and the detergent to be used depending on the weight of the load and the type of fabric. They can also automatically send alerts when the detergent runs out. However, in the energy field, within the framework of Smart Grids (SG), the term "smart" refers to those appliances capable of modulating their electricity demand in response to signal requests from the electrical system. Thus, household appliances could incorporate different Demand Response (DR) strategies. DR has already proven to be a resource that the grid operator can use in several ways to provide system reliability, stability, and security services such as voltage and frequency support. Typically, DR policies can be divided into direct (explicit DR) through aggregation or virtual power plants (VPP), or indirect (implicit DR) [2]. Explicit DR (also called incentive-based DR program) is divided into traditional-based (e.g., direct load control, interruptible pricing) and market-based (e.g., emergency DR programs, capacity programs, demand bidding programs, and ancillary services market programs). On the other hand, implicit DR (sometimes called price-based DR program) refers to the voluntary program in which consumers are exposed to time-varying electricity prices, e.g. time-of-use pricing, critical peak pricing, and real-time pricing. For the appliances, this would materialize into load-shifting strategies, which shift their operating period from peak to off-peak hours, or load-modulation strategies, which directly reduce or avoid energy use during peak hours.

In the context of the SG, technological advances that enable demand-side resource utilization include bilateral grid-device communication, local and centralized smart controllers, IoT-based coordination and negotiation architecture, controlled and communicated SAs [3]. A different solution is represented by what is known as a grid-friendly or Grid-Interactive Appliance controller (GIAC) [4], [5]. A GIAC can monitor the power frequency and shed the appliance after the under-frequency alarm is triggered, to support the stability of the system. The paper [6] proposes to use appliances equipped with GIAC to

This work was supported by the Project IMPROVEMENT under Grant SOE3/P3E0901 cofinanced by the Interreg SUDOE program and the European Regional Development Fund (ERDF). (Corresponding author: Antonio Moreno-Munoz). Joaquin Garrido-Zafra, Aurora Gil-de-Castro, Rafael Savariego-Fernandez, Matias Linan-Reyes and Antonio Moreno-Munoz are with the Electronics and Computers Engineering Department, Universidad de Cordoba, Cordoba 14071, Spain (e-mail: p22gazaj@uco.es; agil@uco.es; p52safer@uco.es; matias@uco.es; a.moreno@ieee.org). Felix Garcia-Torres is with the Electrical Engineering and Automatic control Department, Universidad de Cordoba, Cordoba 14071, Spain (e-mail: fgtorres@uco.es).

address this issue under the umbrella of the IEEE 1547-compliant inverters [7], tripping off-line when operating as part of a microgrid in islanded mode. Finally, the paper [8] introduces a novel approach to establish real-time demand information for a sector of the distribution network. The proposed approach makes it possible to identify the peak and off-peak periods, based on the voltage measured at the electrical panel of the end-users buildings.

Nowadays in many countries, due to the three electricity tariff periods, and the price difference between the off-peak time band compared to the peak time, the electricity over cost when using a normal instead of a responsive appliance is even more visible. As an example, taking into consideration the consumption of a normal appliance as a washing machine[9], it is almost twice the price of using this appliance in one- or another-time band.

Thus, the present work aims to design a new controller that combines both approaches expanding their possibilities: it can act on DR schemes as well as monitor PQ disturbances for the establishment of a wide and eligible range of alarms and restrictions. The idea is also to be connected to the appliance and managed by the EMS according to the presented values. Based on a previous IoT sensor development [10], real-time status information, configuration, consumption data, and even diagnostic data from the appliances can be analyzed and recorded while in operation, and simultaneously transferred to the cloud for machine learning processing.

This paper is a thorough revision of the conference paper [11] focused on PQ that expands the integration of OpenADR [12], [13] together with the IoT flexible devices and platform to deploy protective functionalities according to PQ constraints. This is the main novelty of the present paper, as to our knowledge, there is no previous research combining them all to provide PQ functionalities supporting the power system under anomalies or faults.

The rest of this paper is organized as follows: Section 2 presents a review of the IoT and the OpenADR standard employed. Section 3 is devoted to the design of the controller, including hardware devices employed and their configurations and discussing the communications environment. The main features of the developed IoT platform are stated in Section 4 and the tests are then discussed in Section 5. Finally, the conclusions and future work are reported in Section 6.

II. Overview

A. IoT communication protocols

IoT has become one of the most significant trends in the information and communication technology (ICT) world. IoT applications are proliferating in all industries. Although there is no universal definition, several authors have provided definitions of the term [14], [15], [16]. The general idea refers to all those everyday objects connected to the Internet. Standardization is the current problem with IoT protocols, as there are too many protocols and aspirants to be standardized. While their consolidation is coming, what is currently being created is more confusion with each new device that is launched onto the market. There have been many attempts to review all protocols [17], [18], [19]. In the paper [20], the authors even name the technologies of the future as the 5G. In [21], the author makes a good attempt to classify all existing protocols into layers similar to ISO levels of communications. IEEE 802.15.4 and IEEE 802.15.4e are among the most widespread communication protocols: They define access to the physical layers as well as access control levels for Wireless Personal Area Networks (WPANs), and they are mainly used for networks with low transmission rates and low power consumption. Based on the standard IEEE 802.15.4 of WPAN, ZigBee is a high-level wireless communication protocol, operating at 2.4 GHz and its bandwidth is up to 250 kbps, to be used in ultra-low power wireless communications. LoRaWan [22] is a non-cellular low-power wide-area network (LPWAN) wireless communication network protocol, particularly intended for low power devices. LoRaWAN is mainly used within the IoT for connections among devices. Some characteristics are secure bi-directional, low power consumption, long communication range, low data rates, low transmission frequency, mobility, and location services. SigFox is also a protocol for IoT that rewards low power consumption, 12-byte messages are used and are valid for networks up to 50 km. One of its main advantages is that has compatibility with major manufacturers in the market. Another option is the use of the existing mobile phone network itself, like GSM, UMTS or LTE network. The main advantage is that can use a network that is already in service, while the main disadvantage is the cost of using a network which is not oriented to low consumption.

B. IoT data protocols

The most used IoT data protocols today are as follows: Message Queuing Telemetry Transport (MQTT) (and its variant MQTT-S), Simple Object Access Protocol (SoAP), Constrained Application Protocol (CoAP), Extensible Messaging and Presence Protocol (XMPP), and Representational State Transfer (REST).

The MQTT [23] protocol permits an extremely lightweight publication/subscription messaging model, using Machine to Machine (M2M) communication mainly with a star network topology. Typically used for bi-directional communications in unreliable networks and battery-powered devices with low power consumption. The MQTT-S variant is useful for devices requiring more time on standby mode, allowing up to ten times more scalable devices.

The SoAP was created by the UserLand company in 1998. It oversees structuring the message so that it can be sent from or to the server and put into an Extensible Markup Language (XML) file, an extensible frame language used to store data legibly. As such, it is not tied to or linked to any programming language. It was highly accepted by companies when it came to light, but today it competes against other modern languages. SoAP is an information exchange protocol based on XML, designed for the Internet, and is used to encrypt information from the requirements of Web Services and respond to messages before sending them to the network. SoAP uses Web Service Description Language (WSDL) which is an

independent platform, is an extension of the XML language that stores and locates Web Service applications.

The CoAP protocol is an improved protocol version from MQTT-S oriented to Web Services instead of messages as MQTT. It also provides support for integration and content discovery, sends, and receives UDP packets, and is designed to request and receive information via the hypertext transfer protocol (HTTP) with methods like GET, PUT, POST, and DELETE. It also adapts to the node-sensor format with 8-bit controllers and allows the use of 6loWPAN networks that fragment IPv6 packets into small layer frames.

REST relies on HTTP to exchange information and does not need extra encapsulation to do so. It is lighter and easier to use but with some limitations. Instead of making requests encapsulated in an "envelope SOAP" to request a service for which the WSDL is necessary, in REST the requests are made through the HTTP protocol with GET, POST methods without the need to encapsulate it. It uses a single communication path between the device and the cloud and prioritizes Network Address Translation (NAT) address crossing.

XMPP allows an extensive number of uses, including instant messaging or voice and video calling, redistribution of contents, and generalized routing of XML data. Massive real-time scalability for approximately 100,000 nodes. It is also used when traffic messages are large and potentially complex for each device. Also used when extra security is demanded.

C. OpenADR standard

Several studies have been conducted on OpenADR as a communication data model for automatic DR. For example, the paper [24] introduces a multi-agent system (MAS) that aggregates consumers and prosumers and handles automatically OpenADR-compliant DR requests. The proposed framework ensures a 100% DR success rate through a dynamic, bi-directional DR matchmaking process that can mitigate observed deviations both internally and externally in real-time. Authors use OpenADR as the standard for encoding and communicating, e.g., DR events, energy-related reports, and availability schedules.

The paper [25] studies the layered architecture applied to automatic DR systems and presents an automatic DR hierarchical management system with client-server information interaction pair as the basic unit. In the OpenADR framework, the clients and the server are better known as virtual end nodes (VEN) and virtual top nodes (VTN) respectively, and their roles will be discussed later. The paper [26] proposes the use of the OpenADR standard protocol in combination with a Decentralized Permissioned Market Place (DPMP) based on Blockchain. It shows the result of a real experimental case, which implements a Capacity Bidding Program (CBP) where the OpenADR protocol is used as a communication method to control and monitor energy consumption.

However, less attention has been paid to this concept in combination with IoT. One of the few researchers addresses DR load control in an SG using IoT technology [27]. Authors present the charging control of plug-in electric vehicles in response to real-time pricing from a utility. The Plug-in Electric Vehicle (PEV) charging is coordinated with real-time pricing and desired target State of Charge (SOC). Moreover, authors in [12] propose a solution based on the standard OpenADR, creating a platform based on IoT capable of turning on or off electrical devices based on a central decision process that meets the requirements of energy producers and consumers. Another example is found in [28], where an open-source platform is developed to allow sensing and control of heating, ventilation, and air conditioning (HVAC), lighting, and plug load controllers in small- and medium-sized commercial buildings.

III. GRID-INTERACTIVE APPLIANCE CONTROLLER EXTENDED FUNCTIONALITY

This section describes the proposal of the GIAC shown in Fig. 1. According to this figure, the proposed GIAC includes the prototype board of the IoT PQ sensor besides an infrastructure based on the OpenADR standard. The following lines will describe both elements more in-depth: Firstly, the IoT sensor to monitor PQ and, secondly, the implemented OpenADR infrastructure.

This board includes the input connectors for current (left) and voltage (right) sensing. The current input circuit is intended to be driven by the split-core current transformer SCT 013-030 of YHDC® with a transfer ratio of 30 A/V and the voltage input is connected directly to the power grid. According to the signal conditioning circuits, the board can measure up to 21 A, 460 V, and 9.9 kVA with 2 W maximum power consumption. Moreover, the board was equipped with the thermistor MCP9700A for monitoring the temperature at the measurement point.

The signal acquisition is performed by a specific purpose integrated circuit (IC) for energy measurements. The device selected was the MCP3909. As in previous works [10], [29], [30], the implemented hardware architecture consists of an ESP32 system-on-chip (SoC) that retrieves data from the IC through a Serial Peripheral Interface (SPI) bus. However, in this design, the ESP32 SoC retrieves raw data (current and voltage samples) rather than traditional PQ indices computed by the IC such as the root mean square (RMS) values, Powers, total power factors (TPF), or total harmonic distortions (THD). This means that the workload has been transferred from the IC to the ESP32 SoC aiming to build and compute custom algorithms and PQ indices from the current and voltage waveforms. The waveforms are retrieved with 16 bits resolution from the delta-sigma analog to digital converters (ADCs) at the frequency of 12.8 kHz. As was stated, the ESP32 SoC includes an SPI bus to retrieve the samples provided by the IC, however, this is not the only communication interface: Once the data processing is performed over these waveforms, other communication channels must be set up to connect the board to the infrastructure detailed in section IV. In our research, the communication protocol involved in the data transmission was the MQTT protocol due to their lightweight implementation [31] to be used in low-resources devices with limited bandwidth.

The primary power source of the prototype is the power grid from which it is collecting the measurements. To accomplish this, a step-down transformer and a circuit based on a linear voltage regulator are employed to provide the DC power supply

for the ICs. Also, the board includes an external backup 9 V input that is enabled when the main grid may be unstable (i.e., voltage sags) and is used to supply the ICs and avoid any disconnection or reset.

After the hardware description, the firmware architecture involved in obtaining the PQ indices from the current and voltage samples acquisition to the data transmission is noteworthy. The ESP32 SoC was equipped with the real-time operating system (RTOS) FreeRTOS [32] and organized as it is depicted in the task diagram of Fig. 2. While task 0 performs and queues the PQ indices, tasks 1, 2, and 3 just wake up when there is available data within their queues, verify the connection with the MQTT broker to avoid the loss of data, dequeue the PQ indices from the real-time queues and publish them. Otherwise, the PQ indices are not dequeued and will therefore be published once the connection is re-established. In this scenario, the reconnection functions are also triggered.

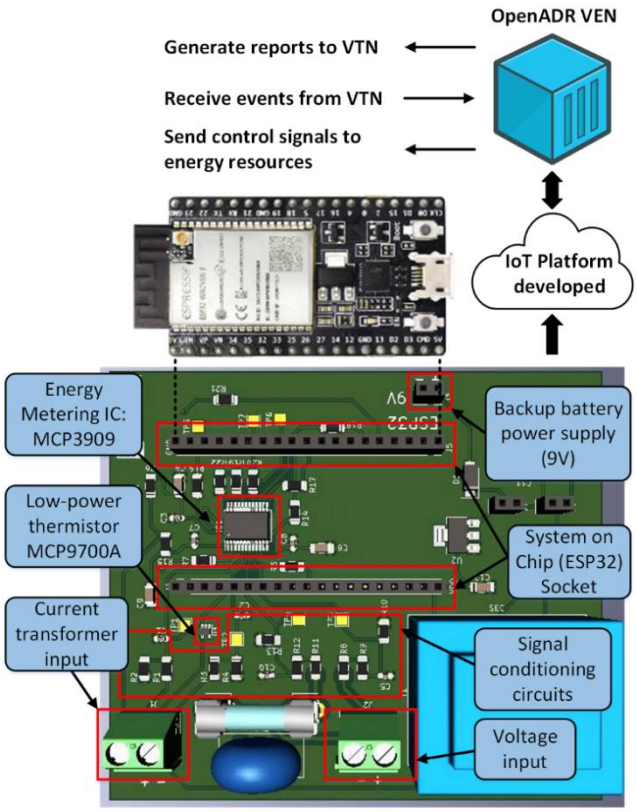

Fig. 1. GIAC overview.

The interrupt service routine (ISR) is triggered once current and voltage samples are converted by the ADCs of the IC. Furthermore, this routine fills up a certain buffer with the previous current and voltage samples and performs the RMS value of the voltage each cycle of the fundamental. Although this RMS value is not reported to the IoT platform, the device uses it internally to assess whether a voltage disturbance has occurred or not with a time response of one cycle of the main grid (approximately 20 ms). If so, the magnitude and duration of such a voltage disturbance are sent to task 1 using the real-time queue 0. As it is also evidenced from Fig. 2, several real-time queues available in FreeRTOS have been included for synchronization purposes between tasks according to the time intervals they are updated. The ISR also uses a wake-up signal to release the highest priority task (task 0) where the main PQ indices are computed with 10 cycles (approximately 200 ms) as stated in IEC 61000-4-30 for European networks. According to this standard, there are three-time aggregation intervals, 150-cycles (3 seconds approximately), 10-min, and 2 hours which are computed by aggregating these periods of 10 cycles. The device computes the following indices: RMS value of the current and voltage; active, reactive, and apparent powers; current and voltage harmonics (up to 50 order), frequency, TPF, and THD for the voltage and current in percent of fundamental of the voltage or current respectively, as well as transients as voltage sags and swells (providing, in this case, their magnitudes and durations), and temperature at the measurement point. All the parameter magnitudes are 150-cycle aggregated except the voltage disturbances which are asynchronously reported due to their asynchronous nature. Moreover, RMS voltage and current values are reported with a 10 min aggregation as well.

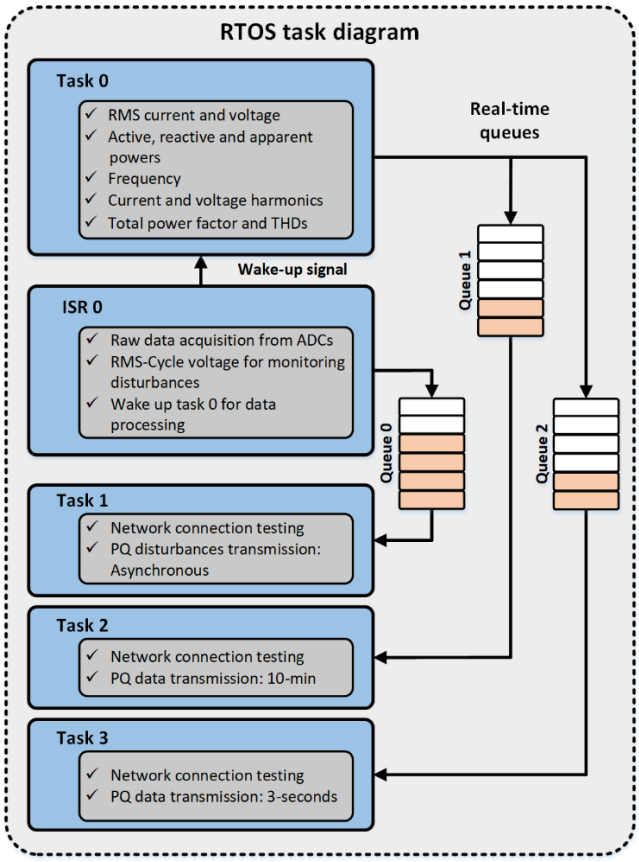

Fig. 2. RTOS task diagram.

Finally, OpenADR has been employed through its python implementation OpenLEADR [33] in this research and has also been deployed over the docker containers technology together with the IoT platform that will be described in section IV. OpenADR enables the development of non-proprietary and standardized interfaces that allow stakeholders in the electricity market (mainly utilities and aggregators) to automatize and simplify the management of the typical DR resources such as

HVAC, lighting, electric water heaters, pool pumps, and factory equipment among others. OpenADR-based entities can send signals and exchange information so that other entities can change their electric load using a common language and the existing communications. As was stated previously in Section II, entities are organized based on a client-server topology in this standard, where clients and servers are better known as VEN and VTN respectively, and their functionality is well-differentiated: The main purpose of VENs is to generate reports that support the VTN decision-making process, as well as receive and acknowledge events from VTN to control the demand side energy resources. By contrast, the VTN has a complete diagnosis of the system whenever it is required thanks to reports delivered by VENs, and can, therefore, create and transmit events to manage the energy resources controlled by them after certain conditions. Although Fig. 1 illustrates the most likely case where a GIAC operates as a VEN, at least one GIAC must operate as a VTN as will be presented in section IV. Regarding the reporting functionality, reports will be focused on PQ and therefore, parameters delivered by VENs are the same described above for the IoT PQ sensor. These reports will be scheduled with a period of approximately 3 seconds. On the other hand, a battery of custom events as well as events based on several standards related to frequency deviations or voltage disturbances will be configured into the VTN.

IV. THE INTERNET OF THINGS PLATFORM DEPLOYED

Once the GIAC has been introduced, the following lines will focus on the IoT platform deployed to collect PQ data to provide monitoring and protective functionality. This Fiware-based platform is shown in Fig. 3 together with the GIACs as well as the laboratory setup configured for the testing process.

At its heart is FIWARE [34] which is an open-source framework that is widely used to speed up and facilitate the development of customized smart solutions for many sectors such as smart city, smart industry, or smart energy. Internally, it uses the next-generation service interface (NGSI) protocol which is aligned with the current ETSI-NGSI specifications and provides communication interfaces called IoT agents for most of the protocols used in IoT (i.e. MQTT, HTTP, LoRaWAN, or Sigfox) as well as seamless integration with third-party applications like popular databases or dashboards to promote interoperability.

For this research, a basic smart solution of six services has been deployed using the container technology provided by docker [35]. These services include the core of any FIWARE-based solution which consists of an instance of the MongoDB database and the so-called orion context broker (OCB) that exchange data through the NGSI protocol as well as with any other container. While this database stores all the defined entities (understood as a thing representation), their attributes structure, and the last value of them even other information related to the relationship between containers, the OCB manages these data. Besides this core, the well-known MQTT broker mosquito has also been used for connecting the IoT PQ sensors as well as the IoT agent for the ultralight 2.0 protocol [36] which is the bridge between the MQTT broker and the OCB to perform the conversion from MQTT to the NGSI protocol. Moreover, the platform also includes a couple of services in charge of managing the time series data: CrateDB and Quantumleap. CrateDB is a Structured Query Language (SQL) distributed database optimized for large-scale IoT projects which makes it suitable for this research due to the large amount of data coming from the sensors. Quantumleap is the connector in charge of persisting the time series data into CrateDB. Finally, the open-source observability platform for data visualization, monitoring, and analysis, Grafana, has also been added.

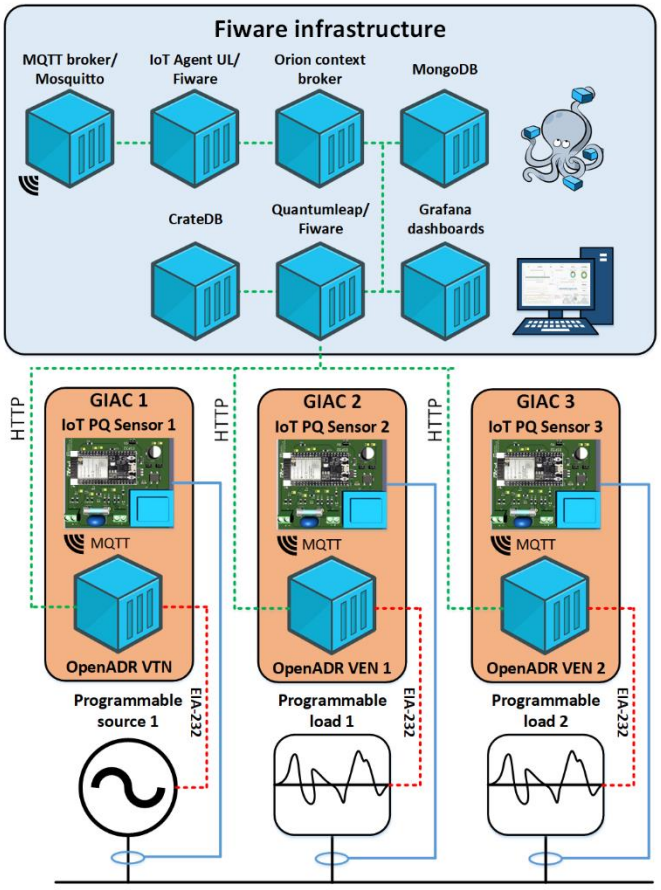

Fig. 3. Block diagram of the IoT platform with the GIAC and the laboratory equipment.

V. PROTECTIVE FUNCTIONALITIES PROVIDED BY THE DEVICES

This section aims to evaluate the effectiveness of the deployed platform and GIACs under several scenarios such as overconsumption, power system frequency deviations, voltage disturbances as well as the presence of certain harmonics or distortion to take corrective or protective actions.

As was stated in section I, this research is focused on the PQ aspects of the power grid and thus, the infrastructure is tested autonomously to evaluate its effectiveness in dealing with PQ deviations without a controller coordinating its operation. Nevertheless, the platform is intended to be driven by a decision-making entity located in the upper layer. In this regard, previous research such as [37], where an EMS for SAs is

This article has been accepted for publication in a future issue of this journal, but has not been fully edited. Content may change prior to final publication. Citation information: DOI 10.1109/TIA.2022.3160410, IEEE Transactions on Industry Applications

developed, or [38], where a load scheduling strategy with PQ constraints is presented, are very suitable for this purpose.

First of all, before discussing the experimental results, a schematic diagram of the corrective action taken by the infrastructure at certain PQ deviations will be presented in Fig. 4. Notice that, when power consumption from each load (P) is over the established limit (P_{max}), the VTN receives the corresponding report and generates the power curtailment event for this load (VEN1 or VEN2) to force it to reduce the consumption up to 98 % of P_{max}. This 2 % hysteresis has been implemented to avoid the VTN is continuously sending power curtailment events. No corrective action is taken if consumption does not exceed P_{max}. Regarding the power system frequency deviations, the balance between total generation and consumption would give a situation with constant frequency. However, this balance might be broken by two reasons: if consumption is over the generation, the frequency falls, and the other way around, it rises when generation is overconsumption. In our research, it is assumed that frequency variations are originated by non-flexible loads while programmable loads 1 and 2 are intended to compensate these deviations according to the following law: if the frequency is over the upper limit (f_{max}), the consumption of this load is then increased in a given percentage of its nominal power. Similarly, when the frequency is below the lower limit (f_{min}), its consumption is decreased by the same percentage. Otherwise, the consumption remains constant at the level at which the frequency is within the limit. So that, the presence of the loads leads to changes in frequency. The values of f_{max} *and* f_{min} have been established according to the standard EN50160 [39] as mentioned below. In case of a voltage disturbance occurrence, the loads will be disconnected from the programmable source whether there is a voltage disturbance that may cause permanent damage to it. To evaluate that, limits defined in standards such as IEEE 1547-2018 [40], IEC 61727-2004 [41], IEEE 929-2000 [42], and VDE 0126-1-1 [43] have been employed so that a voltage disturbance defined with magnitude and duration within the permissible area would be ignored, otherwise, the load would be disconnected. To deal with the presence of voltage harmonics, the infrastructure evaluates the voltage THD as detailed in standards EN 50160 and IEEE 519 [44]. Consequently, the loads are disconnected when the measured THD is over the limits (THD_{max}) defined in such standards. On the other hand, the load returns to its normal operation when this parameter falls below the value THD_{min} (more restrictive than those defined in the standards). As mentioned below, the values THD_{max} and THD_{min} constitute a hysteresis to ensure that the loads' reconnection is performed with an acceptable voltage quality. Finally, the infrastructure also detects which load may be a source of current harmonics or distortion and performs a disconnection to ensure the PQ within the grid. Otherwise, the load behavior is not modified. In this case, the standard IEC 61000-3-2 defines what should or should not be an acceptable current distortion by evaluating the absolute amplitude of the individual current harmonics (I_n). Concretely, the limits ($I_{n\text{-}max}$) defined for SA (class A within the standard) have been employed.

Concerning the experimental results, the test bench of Fig. 5 has been employed. The power system of this laboratory setup includes the programmable power source California Instruments 3001 iX [45] and the programmable load California Instruments 3091LD [46].

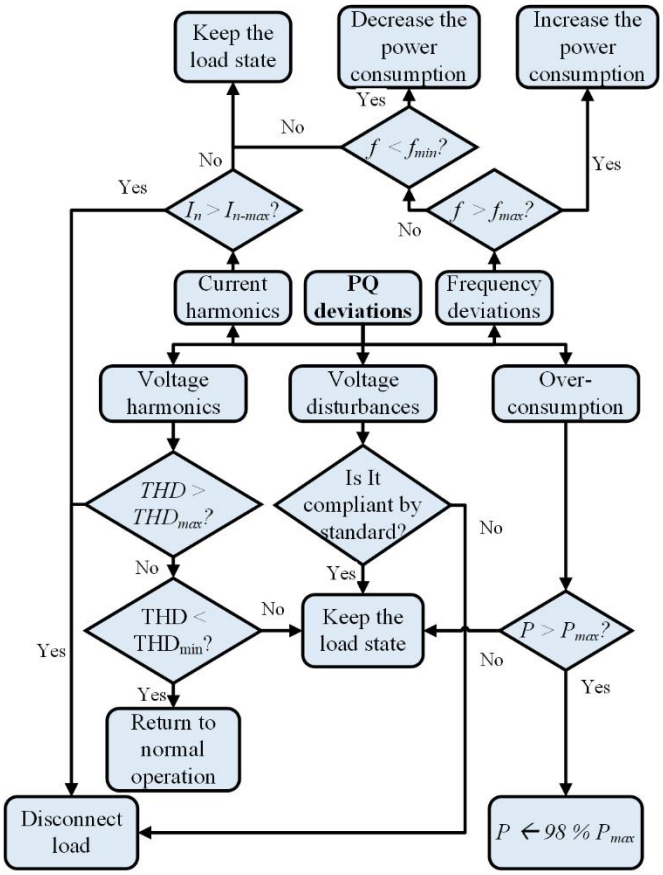

Fig. 4. Schematic diagram of the corrective actions for each PQ deviation.

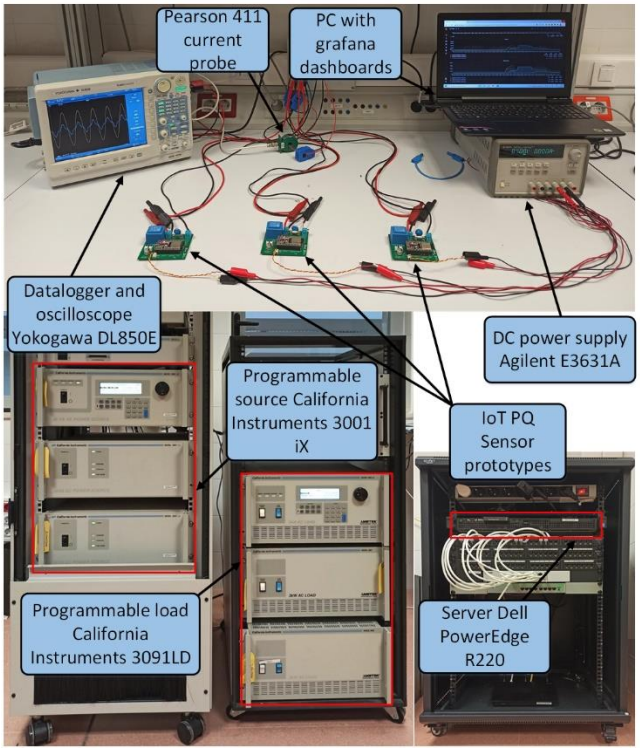

Fig. 5. Laboratory setup.

The server Dell PowerEdge R220 connected to the local network was also used for running the Fiware and OpenADR services, as well as the scripts to control the programmable source and load for the tests. Moreover, the laboratory setup includes the prototypes of the IoT PQ sensors (see Fig. 1) in charge of collecting the measurements shown in the results, and the datalogger and oscilloscope Yokogawa DL850E [47] together with the Pearson 411 [48] current probe for visualization purposes. Finally, the DC power supply Agilent E3631A [49] was also employed as a backup power supply for these boards.

A. Overconsumption

Two tests were accomplished for overconsumption with different power limits, the first test with different power levels for both loads, and the second test with equal power levels. First, Fig. 6 a) introduces the power consumption profiles used as a reference for both programmable loads (loads 1 and 2). These 15 minutes dataset was generated as follows: First, 30 values between 0 and 1.5 kW were randomly generated to ensure that the maximum power of the programmable source was not exceeded, generating 30 seconds duration steps. Then, noise from the standard normal distribution with 0.25 kW of standard deviation was added.

Fig. 6 b) depicts the consumption behavior of loads 1 and 2 (blue and orange lines) when the power limits were set to 1.0 kW and 0.5 kW respectively (see red dashed lines in the figures). The power measured at the voltage source terminal (green line) is also shown. As expected, when power consumptions from each load are over those limits, the load is forced to reduce its consumption up to 98 % of the limit. The power consumption is not modified if it is below the limit. It is noteworthy to mention that as the GIAC computes the active power with 150 cycles of aggregation time (see section III), the corrective actions appear approximately 3-s after the actual change as seen in the spikes of the power consumption when it is over the set limits.

Another test was done, keeping, in this case, the same power limit for both loads. In the case of Fig. 6 c), the limit was set to 1.0 kW. Therefore, the power consumption in load 1 is the same as in the previous test while load 2 is allowed to increase its consumption 0.5 kW more. Likewise, the approximately 3-s response time previously detailed for Fig. 6 a) is also complied in this case as it is derived from the figure.

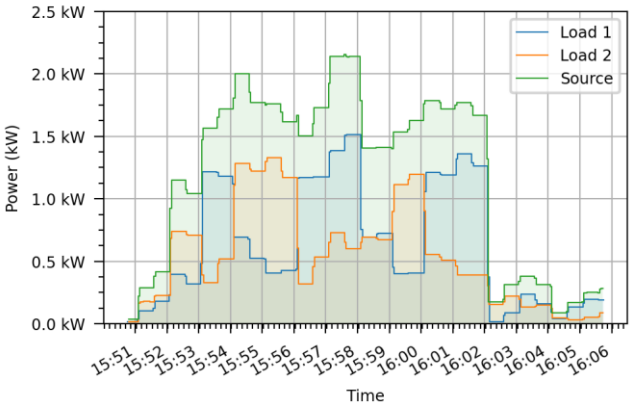

a)

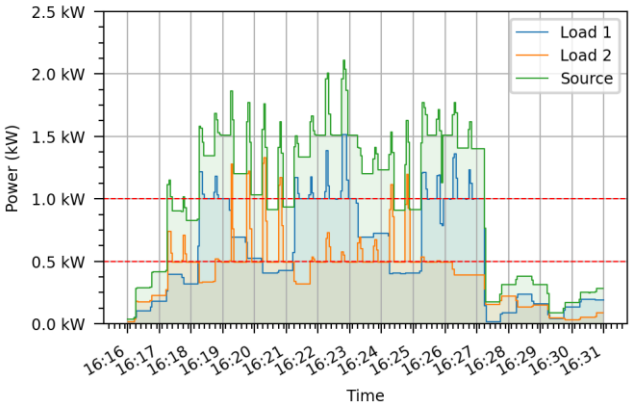

b)

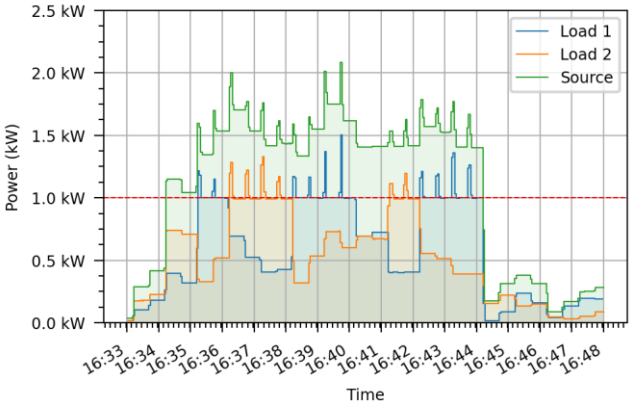

c)

Fig. 6. a) Power profiles employed in the tests as a reference, b) Power consumption when loads 1 and 2 are limited to 1.0 kW and 0.5 kW respectively (Red dashed lines) and c) Power consumption when both loads are limited to 1.0 kW (Red dashed line).

B. Power System Frequency Deviations

Two tests have been carried out for corrective actions related to power system frequency, more specifically, this test accomplishes with standard EN 50160, where the limits for 95 and 100% of the time over a year have been implemented in Fig. 7 a) and b): 49.5-50.5 Hz and 47–52 Hz respectively (see red dashed lines that represent f_{max} and f_{min}) for grid-connected systems.

Although a multitude of PQ disturbances may adversely impact the power system frequency, most of them do so for a very short time and do not depend on the demand side (i.e. voltage disturbances). Therefore, this case study is focused on the steady-state compensation of the frequency deviations by achieving a balance between the total generation and demand of the system. To do so, a couple of flexible loads were employed to modulate the total consumption of the system. Furthermore, the dataset shown in Fig. 7 (see black line) was considered to emulate the influence of non-flexible loads on the frequency. Similar to section A, this dataset was built generating 90 random values varying from 46 to 54 Hz, creating then 10 seconds duration steps with those values, and then, adding noise from the standard normal distribution with 0.5 Hz of standard deviation. As a result, different slopes in the frequency variation have been emulated to test the GIAC under several conditions. Most of the reported frequencies in real

This article has been accepted for publication in a future issue of this journal, but has not been fully edited. Content may change prior to final publication. Citation information: DOI 10.1109/TIA.2022.3160410, IEEE Transactions on Industry Applications

grids are within the limit of 49.5-50.5 Hz, but some points have intentionally been selected to be outside it even reaching 54 Hz or 46 Hz as it has been recorded in a nanogrid in the southern part of Sweden [50]. EN 50160 establishes a larger margin for islanded grids (42.5-57.5 Hz during 100% of the time).

Fig. 7 a) shows the first scenario where the permissible region for the frequency goes from f_{min} = 47 to f_{max} = 52 Hz (red dashed lines). Loads 1 and 2 start from 0.2 and 0.5 kW, respectively, and increase their values with a rate of change of 2 % of their nominal power. Notice that the control rule is successfully applied to compensate the frequency deviations: From 11:42:30 to 11:43:45 the power consumption of both loads keeps growing so that when the frequency is over f_{max}, it can be compensated due to the increase in generation. Something similar but shorter in duration takes place at 11:44:30 and 11:52:15. On the contrary, the frequency falls below f_{min} twice: from 11:46:40 to 11:47:30 and from 11:49:50 to 11:50:25, however, the frequency does not keep below the limit within those intervals which leads to rising the power consumptions with several steps while they keep falling. For the rest of the test, the frequency is within the limits therefore the power on the demand side remains constant.

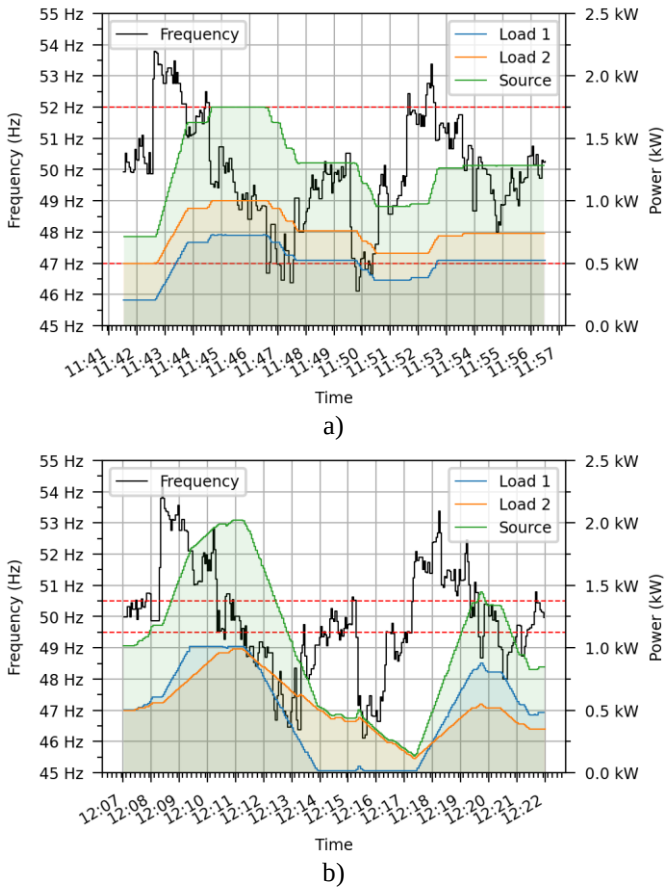

Fig. 7. a) Power consumption for loads 1 and 2 and measured at the source terminal when both loads are employed to compensate power system frequency deviations (47-52 Hz). b) Power consumption for loads 1 and 2 and measured at the source terminal when both loads are employed to compensate power system frequency deviations (49.5-50.5 Hz). Red dashed lines are the limits at EN 50160.

The second scenario is depicted in Fig. 7 b) where the permitted region is more restrictive (f_{min} = 49.5, f_{max} = 50.5 Hz). Accordingly, the power consumption will suffer more variations compared to the previous scenario. Moreover, the initial power has been changed to 0.5 kW for both loads and the ratio of change for load 2 has been changed to 1 %. Note that frequency keeps above f_{max} from 12:08:15 to 12:10:25 and thus, the power consumption does rise, however, immediately load 1 reaches its nominal power while load 2 still does not. In this context, load 1 will opt out of the event transmitted by the VTN as cannot increase its consumption to reach a balance between consumption and generation. Although the period from 12:17:15 to 12:19:30 is similar, the consumption does not reach the nominal power. In contrast, this can also happen when the power system frequency drops below f_{min}. Notice the period from 12:11:20 to 12:14:00 in which the nominal power of load 1 falls up to 0.0 kW and remains constant even when the frequency is still below f_{min} as the disconnection of the power is necessary to keep the frequency.

C. Voltage Disturbances

The voltage disturbances test was performed by generating several voltage sags and swells with different magnitudes and durations using the programmable voltage source. As in the previous tests, the main purpose is to check whether the deployed infrastructure can detect the voltage disturbance events and carry out a certain policy towards the loads.

Nevertheless, a simple test was performed to validate the measurement device before exposing the whole system to a more complex scenario. In this regard, Fig. 8 shows a screenshot of the Tektronix MDO3024 oscilloscope with the voltage and current waveforms of the load fixed at 230 V and 1 A (see red and purple waveforms respectively).

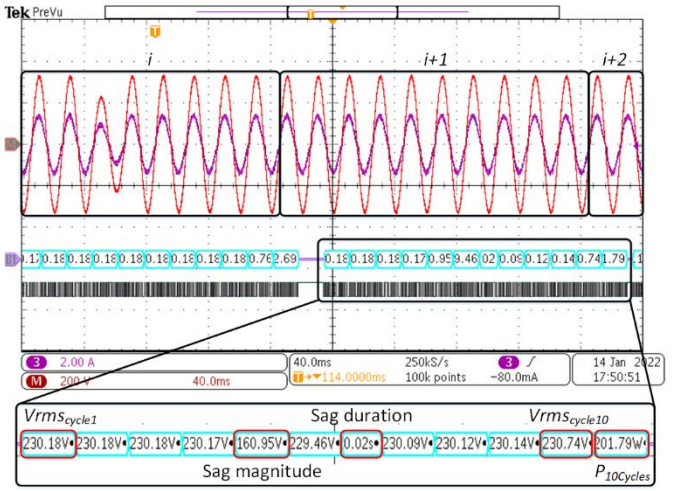

Fig. 8. Load voltage and current, as well as device measurements during a test voltage sag.

These waveforms in the screenshot have been separated in 10-cycle windows (*i*, *i+1*, *i+2*) (note that *i* window is not completed, and two cycles are missing in the left hand side of the screenshot) since the device calculates parameter magnitudes over 10-cycle time interval according to the abovementioned standards. Below these current and voltage waveforms, the decoded frame with the measurements from *i*

window sent by the universal asynchronous receiver transmitter (UART) of the device can be found. It should be mentioned that measurements include the RMS voltage of each cycle of the window ($V_{RMS_{Cycle1}}$, $V_{RMS_{Cycle2}}$…$V_{RMS_{Cycle10}}$), the duration of the voltage disturbance (if any), and the power corresponding to this 10-cycles window ($P_{10Cycles}$) and appear at approximately the same time as the next window ($i+1$) since the device processes a 10-cycles window while acquiring the next one. For a more detailed visualization, this communication frame has been expanded to show the measurements described.

Notice that a voltage sag (160 V and 0.02 s of magnitude and duration) is generated in the fifth cycle of *i* window by the programmable power source and consequently, a voltage sag of 160.95 V and 0.02 s of magnitude and duration respectively was detected by the device as it is derived from the figure. It is noteworthy that the voltage disturbances detection algorithm needs to recognize one cycle where RMS voltage is within the range of 90-110 % of the nominal voltage (230 V in this case) to detect the end of a voltage disturbance, that is why the sag magnitude and duration do not come together in the frame. Finally, an active power of 201.79 W for the *i* window is reported.

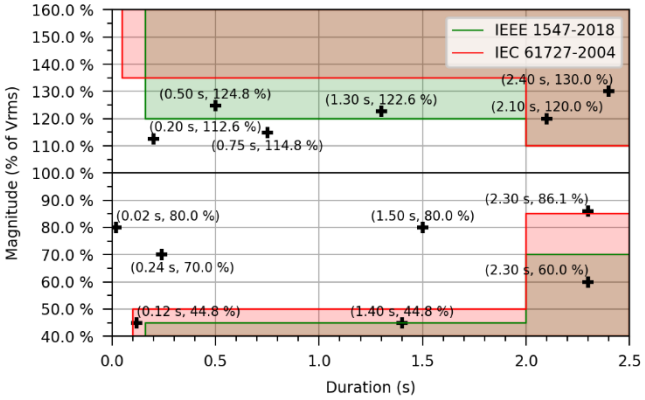

a)

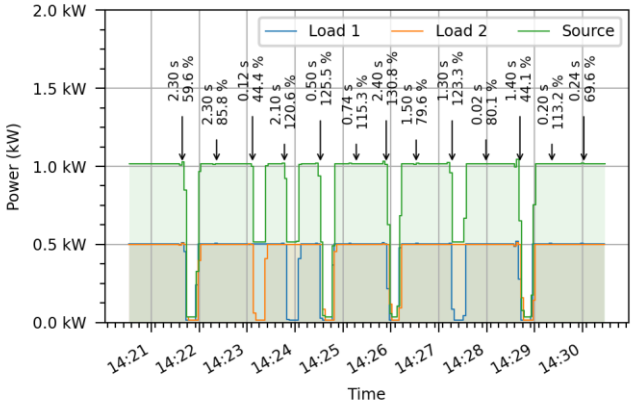

b)

Fig. 9. a) Voltage disturbances configured for scenario 1 and limits defined by standards IEEE 1547-2018 and IEC 61727-2004. The shaded part denotes the prohibited region. b) Voltage disturbances identified by the GIAC and power consumption of loads in scenario 1.

Once this device functionality has been validated, Fig. 9 shows scenario 1 where the standards IEEE 1547-2018 and IEC 61727-2004 have been employed as a reference for loads 1 and 2 respectively. Notice that these standards define different admissible limits or regions (see Fig. 9) and thus different criteria for what should or should not be an allowable voltage disturbance. Consequently, a certain voltage disturbance may cause the disconnection of one load while the other one remains connected since this voltage disturbance is evaluated according to different standards for loads 1 and 2.

Fig. 9 a) depicts the limits established by such standards (green and red areas for both standards) and a battery of thirteen voltage disturbances configured for this experimental test (230.0 V as reference) covering all areas within or outside the limits (crosses in the figure). While the shaded part denotes the prohibited area defined by one or both considered standards, and thus, voltage disturbances located here will cause the loads' disconnection; the remaining blank region between upper and lower limits indicates the safety area, where no actions are taken. Specifically, the voltage sags and swells have been configured to test all possible cases in a 10 min test: Load 1 disconnected, load 2 disconnected, none of them disconnected, and both loads disconnected. Those values have been selected considering the most often registered voltage sags in LV networks in countries reported at [51].

On the other hand, the loads' behavior when these disturbances are applied is depicted in Fig. 9 b). Concretely, both loads were set to a constant power of 0.5 kW for more detailed visualization of the protective actions. Four voltage disturbances with 2.3, 2.1, 2.4, and 1.4 seconds of duration and 60.0, 120.0, 130.0, and 44.8 % of magnitude respectively led to the disconnection of both loads as they belong to shaded green and red areas and their durations and magnitudes were measured with less than 0.0 and 1.34 % of error by the devices. Moreover, five disturbances characterized by 0.75, 1.5, 0.02, 0.2, and 0.24 of duration and 114.8, 80.0, 80.0, 112.6, and 70.0 % of magnitude respectively did not cause the disconnection of any load as they belong to the blank area and were identified with less than 1.34 and 0.572 % of error. Those leading to the disconnection of loads 1 and 2 were detected correctly and also identified with a maximum error of 0.67 and 0.0 % in magnitude and duration.

Similarly, scenario 2 is depicted in Fig. 10, however, the standards IEEE 929-2000 and VDE 0126-1-1 were employed. Another thirteen voltage disturbances were also generated and shown in Fig. 10 a) to ensure that all possible cases abovementioned were tested.

The group of three disturbances that caused the disconnection of both loads –see Fig. 10 b)- was detected correctly and is characterized by 2.2, 2.3, and 1.0 seconds of duration and 70.0, 130.0, and 41.7 % of magnitude respectively. The maximum error was 1.44 and 0.0 % in magnitude and duration in this case. The three voltage disturbances located in the safety region –blank area- (0.75, 0.04, and 0.1 seconds of duration and 112.2, 84.8, and 114.8 % of magnitude) did not trigger any protective functionality as expected and were identified with a maximum error of 1.34 and 0.45 %. Finally, the other seven disturbances characterized by 2.1, 0.15, 0.5, 2.1, 1.6, 1.4, and 0.35 seconds of duration and 84.8, 44.8, 130.0, 112.2, 74.8, 121.7, and 70 % of magnitude (load 1 or load 2 disconnection) were successfully recognized and thus the

protective functionality was triggered. In this latter case, the maximum error was 0.67 and 6.7 % in magnitude and duration.

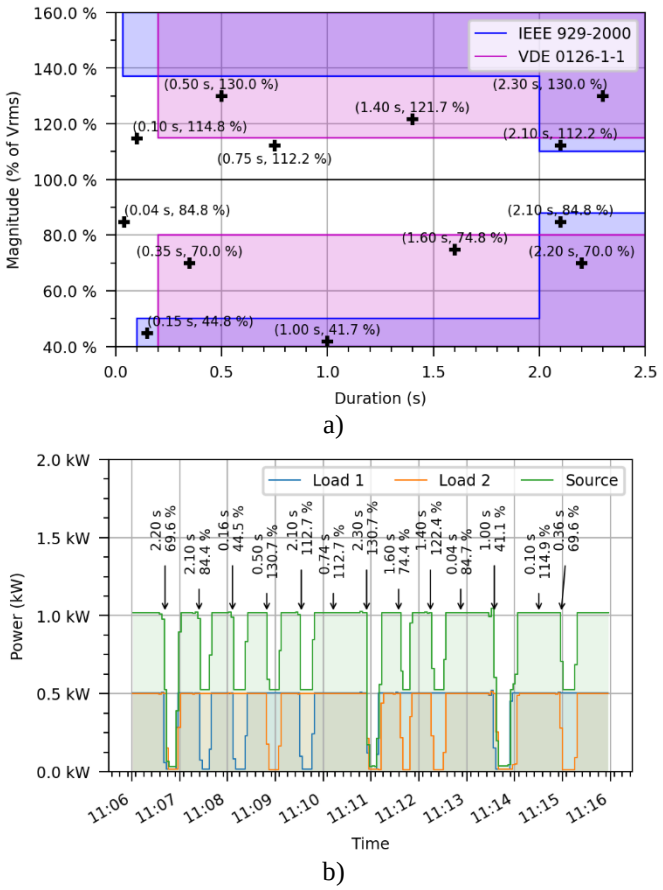

Fig. 10. a) Voltage disturbances configured for scenario 1 and limits defined by standards IEEE 929-2000 and VDE 0126-1-1. The shaded part denotes the prohibited region. b) Voltage disturbances identified by the GIAC and power consumption of loads in scenario 2.

D. *Voltage harmonic distortion*

The voltage harmonic distortion test is presented in this section. As mentioned above, the voltage THD is employed to evaluate the voltage distortion (expressed in percentage of the fundamental). Therefore, the THD profile depicted in Fig. 11 (see black line) has been generated with a duration of 10 minutes from the standard normal distribution (3 % of standard deviation and 7 % of mean) to test the deployed infrastructure. The red dashed lines at 12, 8, and 6 % represent the limits defined by the standards IEEE 519, EN 50160 and the criterion for the load's reconnection respectively. Moreover, the standard IEEE 519 has been applied to load 1 and standard EN 50160 to load 2 and the power consumption was set to 1.0 and 0.5 kW respectively. As in section C, such standards define different limits of THD and thus a certain value of this parameter may cause the disconnection of one load while the other one remains connected.

Fig. 11 also depicts the power consumption of both loads as well as the power measured at the source terminal (see the blue, orange, and green lines respectively). Notice that load 1 is disconnected from the grid at 18:54:45 and 18:59:45 since the voltage THD rises above 12 %. However, load 2 is disconnected when the voltage THD is over 8 % which takes place at 18:52:45, 18:55:45, 18:57:45, 19:00:45 besides the previous instants when load 1 is disconnected since the standard EN 50160 is more restrictive than IEEE 519.

Furthermore, the reconnection of both loads must take place when the voltage THD falls below 6 % as was stated at the beginning of this section. In this regard, instants 18:53:45, 18:55:15, 18:56:45, 18:58:15 and 19:00:30 illustrate examples of this behavior. Given the results, it is possible to verify the effectiveness of the infrastructure.

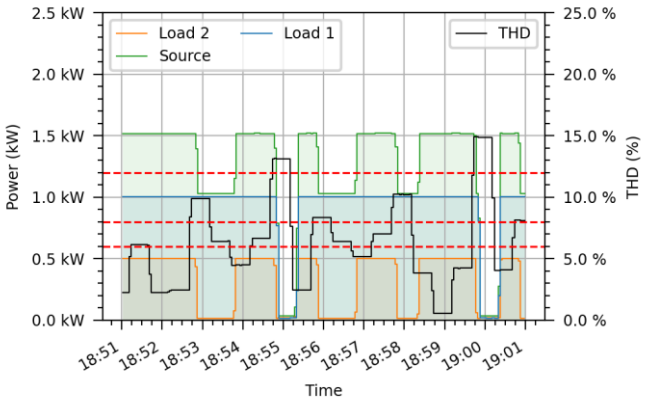

Fig. 11. Voltage THD profile configured for the test, power consumption for loads 1 and 2, and measured at the source terminal. Red dashed lines are the limits defined in IEEE 519 (12 %), EN 50160 (8 %), and the loads' reconnection criterion (6 %).

E. *Current harmonic distortion*

Finally, the performance of the infrastructure when dealing with the presence of current harmonics is reported in this section with a 10 minutes test. As a criterion, the absolute amplitude of the current harmonics up to order 50 has been considered according to the limits established in the standard IEC 61000-3-2. The load control rule could be as complex as setting the load to a low harmonic emission mode or consumption (if applicable) when a certain harmonic amplitude I_n is over the threshold defined in the standard ($I_{n\text{-}max}$) or just disconnecting it in such a situation. Furthermore, the control rule adopted also depends on the dynamic of the load to be controlled and its operation modes. In this research, the load is disconnected from the grid (see the schematic diagram at the beginning of this section) to consider a general case since the key element of the research is the performance of the infrastructure when dealing with current harmonics rather than the development of a load control law. However, different control rules could be implemented due to the flexibility of the platform.

The test current employed is composed of harmonics 3 and 4 and their profiles are shown in Fig. 12 a) (See the green and black lines respectively) and have also been generated from the standard normal distribution with 0.5 and 0.1 A of standard deviation and 2.2 and 0.3 A of mean respectively. The red dashed lines are the limits defined by the standard for the considered harmonics: 2.3 A and 0.43 A respectively. Fig. 12 b) shows in blue the power consumption of the load.

Although the absolute value of the current harmonics is the only criterion employed for making decisions on whether the

behavior of the load should be corrected or not, the THD of the current is also depicted in red for a more detailed view of the experiment. Moreover, notice that this magnitude is expressed as a percentage of the fundamental component (I_1), and therefore, when the load is disconnected, this component approaches zero and the THD increases rapidly regardless of how high the magnitude of the rest of the harmonics is.

As expected, the abovementioned behavior can be appreciated from the results. Notice that the 3rd harmonic is over the limit (2.3 A) at 17:50:00, 17:54:00, 17:56:00, and 17:57:00 while the 4th harmonic does it (limited to 0.43 A) at 17:53:00 and 17:58:00. Given the power consumption, the load is always disconnected from the grid at these instants. Nevertheless, the load remains constant in terms of power consumption when the considered current harmonics are within limits.

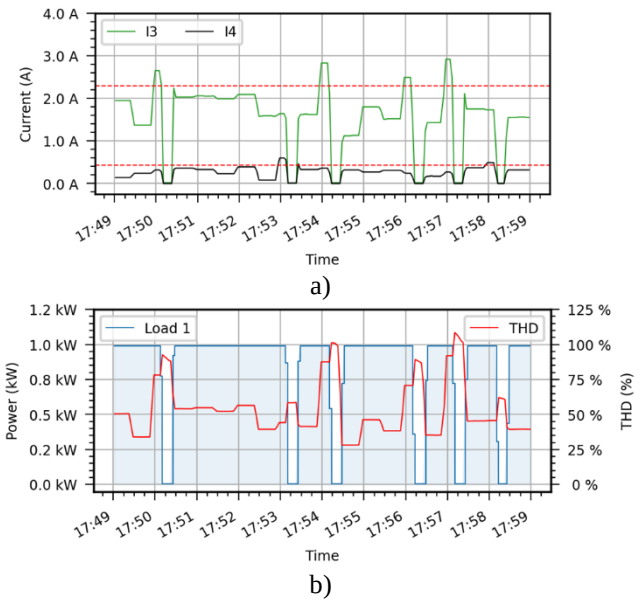

Fig. 12. a) Profiles employed for the 3rd and 4th harmonics and limits defined by the standard IEC 61000-3-2 (red dashed lines), b) Power consumption of load 1 and THD of the current.

VI. CONCLUSION

Responsive appliances are those that, first, represents a significant load that can be reduced, increased, or moved over time, to provide useful support to the power grid, second, provided that the change in its operation is acceptable to the customer, if not imperceptible, and third, can respond to price, demand, or certain grid conditions. This paper resolves many of the technical issues related to the design and construction of these devices, presenting a universal and ambivalent solution as demonstrated by the high-end IoT device, which can communicate and respond to information from the external environment within the framework of a cloud platform. While there are social, political, and economic barriers to the widespread acceptance and adoption of these flexible loads in the marketplace, they need to be addressed and reasonable approaches to overcome them.

REFERENCES

[1] "Household Appliances Report 2019 - Major Appliances Statista Consumer Market Outlook - Segment Report." https://www.statista.com/study/48881/household-appliances-report-major-appliances/ (accessed Nov. 27, 2019).

[2] Z. Ma, J. Billanes, and B. Jørgensen, "Aggregation potentials for buildings—business models of demand response and virtual power plants," *Energies*, vol. 10, no. 10, p. 1646, 2017.

[3] H. Tang, S. Wang, and H. Li, "Flexibility Categorization, Sources, Capabilities and Technologies for Energy-Flexible and Grid-Responsive Buildings: State-of-The-Art and Future Perspective," *Energy*, p. 119598, 2020.

[4] Y.-Q. Bao and Y. Li, "FPGA-based design of grid friendly appliance controller," IEEE Trans. Smart Grid, vol. 5, no. 2, pp. 924–931, 2014.

[5] D. J. Hammerstrom *et al.*, "Pacific northwest gridwise™ testbed demonstration projects; part ii. grid friendly™ appliance project," Pacific Northwest National Lab.(PNNL), Richland, WA (United States), 2007.

[6] K. P. Schneider et al., "Enabling resiliency operations across multiple microgrids with grid friendly appliance controllers," IEEE Trans. Smart Grid, vol. 9, no. 5, pp. 4755–4764, 2017.

[7] R. Real-Calvo, A. Moreno-Munoz, V. Pallares-Lopez, M. J. Gonzalez-Redondo, I. M. Moreno-Garcia, and E. J. Palacios-Garcia, "Intelligent Electronic System to Control the Interconnection between Distributed Generation Resources and Power Grid," RIAI - Rev. Iberoam. Autom. e Inform. Ind., vol. 14, no. 1, 2017, doi: 10.1016/j.riai.2016.11.002.

[8] C. Guzman, A. Cardenas, and K. Agbossou, "Local estimation of critical and off-peak periods for grid-friendly flexible load management," *IEEE Syst. J.*, vol. 14, no. 3, pp. 4262–4271, 2020.

[9] M. Bilton *et al.*, "Impact of energy efficient appliances on network utilisation," *Rep. C2 "Low Carbon London" LCNF Proj. Imp. Coll. London*, 2014.

[10] Medina-Gracia et al., "Power Quality Sensor for Smart Appliance's Self-Diagnosing Functionality," IEEE Sens. J., vol. 19, no. 20, pp. 1558–1748, 2019, doi: 10.1109/JSEN.2019.2924574.

[11] J. Garrido-Zafra, A. Gil-de-Castro, R. Savariego-Fernandez, M. Linan-Reyes, A. Moreno-Munoz, and F. García-Torres, "A Novel Microgrid Responsive Appliance Controller," in *2020 IEEE International Conference on Environment and Electrical Engineering and 2020 IEEE Industrial and Commercial Power Systems Europe (EEEIC/I&CPS Europe)*, 2020, pp. 1–6.

[12] J. Ferreira, H. Martins, M. Barata, V. Monteiro, and J. L. Afonso, "OpenADR—intelligent electrical energy consumption towards internet-of-things," in *CONTROLO 2016*, Springer, 2017, pp. 725–736.

[13] "OpenADR." https://www.openadr.org/ (accessed Jun. 23, 2021).

[14] L. Atzori, A. Iera, and G. Morabito, "The internet of things: A survey," *Comput. networks*, vol. 54, no. 15, pp. 2787–2805, 2010.

[15] D. Bandyopadhyay and J. Sen, "Internet of things: Applications and challenges in technology and standardization," *Wirel. Pers. Commun.*, vol. 58, no. 1, pp. 49–69, 2011.

[16] B. Hammi, R. Khatoun, S. Zeadally, A. Fayad, and L. Khoukhi, "IoT technologies for smart cities," *IET Networks*, vol. 7, no. 1, pp. 1–13, 2017.

[17] O. Alvear, C. Calafate, J.-C. Cano, and P. Manzoni, "Crowdsensing in smart cities: overview, platforms, and environment sensing issues," *Sensors*, vol. 18, no. 2, p. 460, 2018.

[18] A. J. C. Trappey, C. V Trappey, U. H. Govindarajan, A. C. Chuang, and J. J. Sun, "A review of essential standards and patent landscapes for the Internet of Things: A key enabler for Industry 4.0," *Adv. Eng. Informatics*, vol. 33, pp. 208–229, 2017.

[19] P. P. Ray, "A survey on Internet of Things architectures," *J. King Saud Univ. Inf. Sci.*, vol. 30, no. 3, pp. 291–319, 2018.

[20] S. K. Goudos, P. I. Dallas, S. Chatziefthymiou, and S. Kyriazakos, "A survey of IoT key enabling and future technologies: 5G, mobile IoT, sematic web and applications," *Wirel. Pers. Commun.*, vol. 97, no. 2, pp. 1645–1675, 2017.

[21] A. Passemard, "The Internet of Things Protocol stack – from sensors to business value | Internet of Things (IoT) talks." https://entrepreneurshiptalk.wordpress.com/2014/01/29/the-internet-of-thing-protocol-stack-from-sensors-to-business-value/ (accessed Jan. 16, 2019).

[22] W. Ayoub, A. E. Samhat, F. Nouvel, M. Mroue, and J.-C. Prévotet, "Internet of Mobile Things: Overview of LoRaWAN, DASH7, and NB-IoT in LPWANs standards and Supported Mobility," *IEEE Commun. Surv. Tutorials*, 2018.

[23]A. Banks, E. Briggs, K. Borgendale, and R. Gupta, "MQTT." 2018, [Online]. Available: http://docs.oasisopen.org/mqtt/mqtt/v5.0/mqtt-v5.0.html.
[24]C. Patsonakis *et al.*, "Optimal, dynamic and reliable demand-response via OpenADR-compliant multi-agent virtual nodes: Design, implementation & evaluation," *J. Clean. Prod.*, p. 127844, 2021.
[25]Z. Jingxi, C. Min, W. Ling, Y. Lixia, P. Shixiong, and L. Dong, "Research on Architecture of Automatic Demand Response System Based on OpenADR," in *2018 China International Conference on Electricity Distribution (CICED)*, 2018, pp. 2984–2988.
[26]J. I. Guerrero Alonso *et al.*, "Flexibility Services Based on OpenADR Protocol for DSO Level," *Sensors*, vol. 20, no. 21, p. 6266, 2020.
[27]P. Aggarwal, B. Chen, and J. Harper, "Integration of OpenADR with node-RED for demand response load control using Internet of things approach," SAE Technical Paper, 2017.
[28]M. Pipattanasomporn, M. Kuzlu, W. Khamphanchai, A. Saha, K. Rathinavel, and S. Rahman, "BEMOSS: An agent platform to facilitate grid-interactive building operation with IoT devices," in *2015 IEEE Innovative Smart Grid Technologies-Asia (ISGT ASIA)*, 2015, pp. 1–6.
[29]M. Alonso-Rosa, A. Gil-de-Castro, R. Medina-Gracia, A. Moreno-Munoz, and E. Cañete-Carmona, "Novel Internet of Things Platform for In-Building Power Quality Submetering," *Appl. Sci.*, vol. 8, no. 8, p. 1320, Aug. 2018, doi: 10.3390/app8081320.
[30]M. Alonso-Rosa, A. Gil-de-Castro, A. Moreno-Munoz, J. Garrido-Zafra, E. Gutierrez-Ballesteros, and E. Cañete-Carmona, "An IoT Based Mobile Augmented Reality Application for Energy Visualization in Buildings Environments," *Appl. Sci.*, vol. 10, no. 2, p. 600, Jan. 2020, doi: 10.3390/app10020600.
[31]"async-mqtt-client/2.-API-reference.md at master · marvinroger/async-mqtt-client · GitHub." https://github.com/marvinroger/async-mqtt-client/blob/master/docs/2.-API-reference.md (accessed Jun. 23, 2021).
[32]"FreeRTOS - Market leading RTOS (Real Time Operating System) for embedded systems with Internet of Things extensions." https://www.freertos.org/ (accessed Jun. 23, 2021).
[33]"Welcome to OpenLEADR — OpenLEADR 0.5.24 documentation." https://openleadr.org/docs/index.html (accessed Jun. 23, 2021).
[34]"FIWARE." https://www.fiware.org/ (accessed Nov. 27, 2019).
[35]"Enterprise Container Platform | Docker." https://www.docker.com/ (accessed Nov. 27, 2019).
[36]"GitHub - telefonicaid/iotagent-ul: IoT Agent for a UltraLight 2.0 based protocol (with HTTP, MQTT and AMQP transports)." https://github.com/telefonicaid/iotagent-ul (accessed Jul. 30, 2021).
[37]J. Garrido-Zafra, A. Moreno-Munoz, A. Gil-De-Castro, E. J. Palacios-Garcia, C. D. Moreno-Moreno, and T. Morales-Leal, "A novel direct load control testbed for smart appliances," *Energies*, vol. 12, no. 17, 2019, doi: 10.3390/en12173336.
[38]J. Garrido-Zafra, A. Moreno-Munoz, A. R. Gil-de-Castro, F. J. Bellido-Outeirino, R. Medina-Gracia, and E. Gutiérrez-Ballesteros, "Load Scheduling Strategy to Improve Power Quality in Electric-Boosted Glass Furnaces," *IEEE Trans. Ind. Appl.*, vol. 57, no. 1, pp. 953–963, 2020.
[39]"UNE-EN 50160:2011/A2:2020 Voltage characteristics of electricity supplied by public electricity networks." https://www.une.org/encuentra-tu-norma/busca-tu-norma/norma/?c=N0064209 (accessed Nov. 15, 2021).
[40]A. Moreno-Muñoz, M. González, M. Liñán, and J. J. González, "Power quality in high-tech plants: A case study," in *IEEE Compatibility in Power Electronics 2005*, 2005, vol. 2005, doi: 10.1109/CPE.2005.1547542.
[41]"IEC 61727:2004 Photovoltaic (PV) systems - Characteristics of the utility interface." https://webstore.iec.ch/publication/5736 (accessed Nov. 16, 2021).
[42]"IEEE 929-2000 - IEEE Recommended Practice for Utility Interface of Photovoltaic (PV) Systems." https://standards.ieee.org/standard/929-2000.html (accessed Nov. 16, 2021).
[43]"DIN VDE V 0126-1-1:2013-08 - Automatic disconnection device between a generator and the public low-voltage grid." https://www.vde-verlag.de/standards/0100178/din-vde-v-0126-1-1-vde-v-0126-1-1-2013-08.html (accessed Nov. 16, 2021).
[44]A. Gil-De-Castro, S. K. Rönnberg, M. H. J. Bollen, and A. Moreno-Muñoz, "Study on harmonic emission of domestic equipment combined with different types of lighting," *Int. J. Electr. Power Energy Syst.*, vol. 55, 2014, doi: 10.1016/j.ijepes.2013.09.001.
[45]Ametek Programmable Power, "AC Power Sources i-iX Series II." .
[46]Ametek Programmable Power, "Electronic Loads." .
[47]"DL850E/DL850EV ScopeCorder | Yokogawa Test & Measurement Corporation." https://tmi.yokogawa.com/solutions/discontinued/dl850edl850ev-scopecorder/ (accessed Nov. 15, 2021).
[48]"Pearson Electronics Model 411 Clamp On Current Monitors." https://www.pearsonelectronics.com/products/wideband-current-monitors (accessed Nov. 15, 2021).
[49]"E3631A 80W Triple Output Power Supply, 6V, 5A & ±25V, 1A | Keysight." https://www.keysight.com/es/en/product/E3631A/80w-triple-output-power-supply-6v-5a--25v-1a.html (accessed Nov. 15, 2021).
[50]J. Nömm, S. Rönnberg, and M. Bollen, "An Analysis of Frequency Variations and its Implications on Connected Equipment for a Nanogrid during Islanded Operation," *Energies*, vol. 11, no. 9, p. 2456, Sep. 2018, doi: 10.3390/en11092456.
[51]"The 5th CEER Benchmarking Report on the Quality of Electricity Supply (2011)."

Joaquin Garrido-Zafra (Student member, IEEE) received the MSc degree in Distributed Renewable Energies (2018) and the degree in Industrial Electronics Engineering (2017) from the University of Cordoba (Spain). He is a Professor at the Department of Electronics and Computer Engineering of the same University, and a member of the research group of Industrial Electronics and Instrumentation (IEI). Since 2018, he has participated in several R&D projects obtained in national and international competitive public grants. His research interests are focused on power quality, internet of things, electronic instrumentation, energy management, and the development of embedded systems to be used in smart grids. He is also the author and co-author of numerous conferences and journal papers.

Aurora R. Gil-de-Castro (Senior member, IEEE) received the B.Sc. degree in industrial electronics and automatic engineering and Ph.D. degree in engineering and technology from the University of Cordoba, Cordoba, Spain, in 2009 and 2012, respectively. She is currently an Associate Professor with the Department of Electronics and Computer Engineering, Universidad de Córdoba, Spain. She has authored/coauthored several papers in journals and international conferences. She has been involved in research projects at a local and state level. Her research interests include smart grids, Internet of Things and power quality, more concretely, low- and high-frequency harmonics on domestic equipment, and lighting.

Rafael Savariego-Fernandez received a degree in Industrial Electronic Engineering (2020) from the University of Cordoba (Spain). He is a student of the Master in Distributed Renewable Energies and a member of the Industrial Electronics and Instrumentation research group (IEI). His research interests focus on electronic instrumentation, cybersecurity applied to IoT devices, system administration and PCB design.

Matias Linan-Reyes received a degree in Applied Physical Sciences (Electronics) from the University of Seville, Spain, in 1995. He is a Professor at the Department of Electronics and Computer Engineering of the University of Cordoba, Spain, and a member of the research group Industrial Electronics and Instrumentation (IEI) in energy management and Smart Grid. His research interests focus on electronic instrumentation, electronic systems and design, sensors, Internet of Things, modeling, prediction, and machine learning. He has participated in numerous research projects at the National Institute of Microelectronics in Seville and the University of Cordoba. He is the author and co-author of numerous conference and journal articles, books, and patents.

Felix Garcia-Torres received his Ph.D in Industrial Engineering in December 2015 from the University of Seville, Spain. Currently, he works as assistant professor in the Electrical Engineering Department of the University of Córdoba. Prior to this, he worked for the Spanish National Center on Hydrogen for more than 12 years as Responsible of the Microgrids Laboratory. Previously, he was working in several research centers or technological companies such as the Instituto de Automatica Industrial-Consejo Superior de Investigaciones Cientificas (Spain), the University of Seville spin-off GreenPower Technologies (Spain) and the Université Catholique de l'Ouest (Angers, France). His current research interests are advanced power electronics and control to introduce energy storage technologies in the smart grid. He is co-author of the book Model Predictive Control of Microgrids, Ed. Springer.

Antonio Moreno-Munoz (Senior member, IEEE) is a Professor at the Department of Electronics and Computer Engineering, Universidad de Córdoba, Spain where he is the Chair of the Industrial Electronics and Instrumentation R&D Group. He received his Ph.D. and M.Sc. degrees from UNED, Spain in 1998 and 1992, respectively. From 1981 to 1992 he was with RENFE maintenance service, the Spanish National Railways Company, where he received a scholarship for his university studies. Since 1992 he has been with the University of Cordoba, where he has been the director of its department, and academic director of the Master in Distributed Renewable Energies. His research focuses on Smart Cities, Smart Grids, Power Quality, Internet of energy. He has participated in 22 R&D projects and/or contracts and has more than 200 publications on these topics.
He is currently a Member of European Technology & Innovation Platforms (ETIP) Smart Networks for Energy Transition (SNET) WG-4. WG Member of the Spanish Railways Technological Platform (PTFE). WG Member of the IEEE P3001.9 Recommended Practice for the Lighting of Industrial and Commercial Facilities. Member of the Technical Committee on Smart Grids of the IEEE Industrial Electronics Society. He has been a member of the CIGRÉ/CIRED JWG-C4.24 committee "Power Quality and EMC Issues associated with future electricity networks". He has been a member of the IEC/CENELEC TC-77/SC-77A/WG-9 committee. He has been a member of the ISO International Organization for Standardization AEN/CTN-208/SC-77-210. He is an evaluator of R&D&I projects for the Estonian Research Council, the Fund for Scientific and Technological Research (FONCYT) of the National Agency for the Promotion of Science and Technology in Argentina, and the Directorate General of Research, Development, and Innovation of the Ministry of Science, Innovation, and Universities of Spain, and academic promotion at Qatar University. He is also an evaluator for European Quality Assurance (EQA) and DNV-GL.
Section Board Member in Electronics journal MDPI. Associate Editor in Elsevier's e-Prime journal, Section Editor in Chief in Smart Cities journal MDPI. Associate editor in Electronics journal MDPI. Editor in Intelligent Industrial Systems Journal (Springer Nature Science), Frontiers in Energy Research, Sustainable Energy Systems, and Policies. In addition to the guest editor and reviewer of numerous journals of IEEE, IET, MDPI, and Elsevier.